Journal of Nuclear Materials 402 (2010) 162–166

Contents lists available at ScienceDirect

Journal of Nuclear Materials

journal homepage: www.elsevier.com/locate/jnucmat

Effects of grain refinement on internal oxidation of Alloy 617

Tae Sun Jo [a], Se Hoon Kim [a], Dae-Gun Kim [a], Ji Yeon Park [b], Young Do Kim [a,*]

[a] Department of Materials Science and Engineering, Hanyang University, Seoul 133-791, Republic of Korea
[b] Nuclear Materials Research Center, Korea Atomic Energy Research Institute, Daejeon 305-353, Republic of Korea

ARTICLE INFO

Article history:
Received 27 March 2010
Accepted 13 May 2010

ABSTRACT

The effects of grain size refinement on the internal oxidation behavior of Alloy 617 were investigated by exposure at 950 °C up to 2000 h in He. As-received (AR) and grain-refined (GR) Alloy 617 were oxidized forming Cr_2O_3 as an external oxide scale and Al_2O_3 as an internal oxide. The average depth of the internal oxide formed along the grain boundary in the GR sample was approximately half of that in the AR. The internal oxide in the GR sample was densely stretched by grain refinement because internal oxidation took place mainly along grain boundaries. These differences in internal oxidation behavior affected crack propagation under tensile stress. The longer internal oxides in AR induced rapid crack propagation by a relatively higher stress concentration resulting in larger cracks along the grain boundary, while a number of short cracks located near the surface were observed in GR. Thus, crack propagation was restricted in GR by the even distribution of stress and reduction of stress concentration because of the densely stretched internal oxide.

1. Introduction

Among Generation IV reactor concepts, high temperature gas-cooled reactors (HTGRs) are high-efficiency systems designed for the economical production of hydrogen and electricity. Intermediate heat exchangers (IHX) and hot gas ducts (HGD) in HTGRs are commonly operated at pressure greater than 8 MPa and temperatures higher than 950 °C. Further, the He coolant used in HTGRs contains some impurities such as H_2, H_2O, CO, CO_2, and CH_4. All of these factors make the choice of material for IHXs and HGDs challenging. Alloy 617 is a solid-solution strengthening Ni-based superalloy that shows excellent strength, creep-rupture strength, and oxidation resistance at high temperatures [1,2]. Thus, it is a desirable candidate for tube material of IHX and HGD in HTGRs [3,4].

In Alloy 617, chromium (Cr) and aluminum (Al) are alloyed for the formation of a surface layer to protect against degradation at high temperatures [5]. There have been many studies of the oxidation behavior of this alloy from the view-points of microstructural modifications [6,7], operating atmospheres [8,9], and aging temperatures [10,11]. Most reports were focused on the external oxide scale while internal oxidation has not been discussed in detail in spite of its importance relative to mechanical properties. Generally, cracks under external tensile stress are initiated at defects (like internal oxides) by stress concentration [12].

Fine grains enhance mechanical properties at room temperature. However, at high temperatures, enlarged grain boundary areas in fine grains promote grain boundary sliding, which causes deterioration in mechanical properties such as creep resistance [13]. From the same point of view, the grain size is related to internal oxidation at high temperature; specifically, smaller grains provide more diffusion paths for alloying elements and oxygen. In addition, grain boundaries can play a role as internal oxidation sites during high temperature aging [9,14]. Thus, the grain size of an alloy directly affects its internal oxidation behavior.

In this study, alloys of two different grain sizes were employed for the observation of internal oxidation behavior at high temperature and its effect on mechanical properties. Internal oxidation behavior for alloys of two different grain sizes was demonstrated with associated changes in internal oxide depth, internal oxide area, and Al-depleted zone. The mechanical properties of these thermally degraded alloys were related to crack propagation at the internal oxides.

2. Experimental procedures

The chemical composition of as-received Alloy 617 with average grain sizes of approximately 71 μm is presented in Table 1. Specimens were machined to dimensions of 50 × 30 × 10 mm^3 and then were cold-rolled up to 50% at room temperature. The cold rolling process resulted in grain elongation to an aspect ratio of around 6. Cold-rolled specimens were recrystallized at 1050 °C for 1 h in an Ar atmosphere, thereby reducing the grain size to 5.2 μm. Two types of alloys, as-received (AR) and grain-refined (GR) Alloy 617, were

* Corresponding author. Address: Department of Materials Science and Engineering, Hanyang University, 17 Haengdang-dong, Seongdong-ku, Seoul 133-791, Republic of Korea. Tel.: +82 2 2220 0408; fax: +82 2 2220 4230.
E-mail address: ydkim1@hanyang.ac.kr (Y.D. Kim).

0022-3115/$ - see front matter © 2010 Elsevier B.V. All rights reserved.
doi:10.1016/j.jnucmat.2010.05.013

Table 1
Chemical composition of Alloy 617 (wt.%).

	C	Ni	Fe	Si	Mn	Co	Cr	Ti	P	S	Mo	Al	B	Cu
Max	0.08	53.16	1.49	0.06	0.11	11.58	22.16	0.35	0.003	0.001	9.8	1.12	0.002	0.08

exposed at 950 °C up to 2000 h in a He atmosphere which included impurities such as O_2 (<0.45 vppm), N_2 (<1.45 vppm), total hydrocarbon (THC) (<0.45 vppm), and H_2O (<3 vppm). Microstructures were observed by scanning electron microscopy (SEM) equipped with a back-scattered electron detector (BSE). In addition, each sample was analyzed via electron probe micro-analysis (EPMA). The homogeneity of internal oxide formed by aging for 2000 h was evaluated by the Vickers hardness test, which was performed 100 times for each sample. The 3-point bending test was carried out at a cross head speed of 0.1 mm/min and a displacement of 2 mm for samples aged at 950 °C for 120 h.

3. Results and discussion

3.1. Microstructural characterization

Fig. 1 presents cross-sectional micrographs of AR and GR after exposure at 950 °C for 120 h and 2000 h in the He atmosphere. It is well known that the oxide layer is composed of the external oxide scale (Cr_2O_3) on the surface and the internal oxide (Al_2O_3) along the grain boundaries [9,14–16]. External oxide scale is formed by oxidation of Cr, which diffused out from the alloy matrix, with oxygen supplied from the He atmosphere. The formation of the Cr_2O_3 external oxide scale induced a Cr-depleted zone below the scale.

The internal oxide spread along the grain boundaries via branch-like growth because the internal oxidation took place mainly along the grain boundaries, as presented in Fig. 1. In AR, which has larger grains, the internal oxide was formed deep in the matrix. On the other hand, the depth of internal oxides in GR, which has smaller grains, was relatively shallow in near surface. The branches of the internal oxide were densely stretched because of grain refinement, wherein branches are very close to each other.

The average depth of the internal oxide increased with prolonged exposure time, as plotted in Fig. 2a. The extension of the internal oxide depth in GR was approximately half of that in AR. Fig. 2b illustrates the change in internal oxide area calculated via image analyzer, which is regarded as the amount of internal oxide per unit area. In the case of GR, the internal oxide area at initial exposure increased rapidly compared to that of AR. By prolonged exposure, the rate of internal oxidation in GR gradually decreased, while it was constantly maintained in AR. As a result, the area of internal oxide in AR at 1000 h was almost the same as that of GR, and then it became larger than that of GR.

Such an internal oxidation rate depends on diffusion of elements such as Al from the matrix and oxygen (O) from the environment. Internal oxidation rate at initial exposure was fast because of the steady supply of elements such as Al and O. Not surprisingly, the formation of the internal oxide as Al_2O_3 results in the evolution of an Al-depleted zone in the matrix toward the depth, which is defined as a region with lower Al concentration than average in the matrix. The Al-depleted zone was expanded by the continuous internal oxidation during the aging. Thus, the more internal oxidation progressed for longer exposure, the more Al diffusion distance from the matrix to internal oxidation region. Consequently, the internal oxidation becomes slow and depends on diffusion kinetics. The internal oxidation rate is directly related to the mass flux (J) of diffusion driven by the Al concentration gradient (dc/dx). Fig. 3 presents the relative amount of Al concentration profile from the starting point ($x = 0$) at the end of the internal oxidation region to-

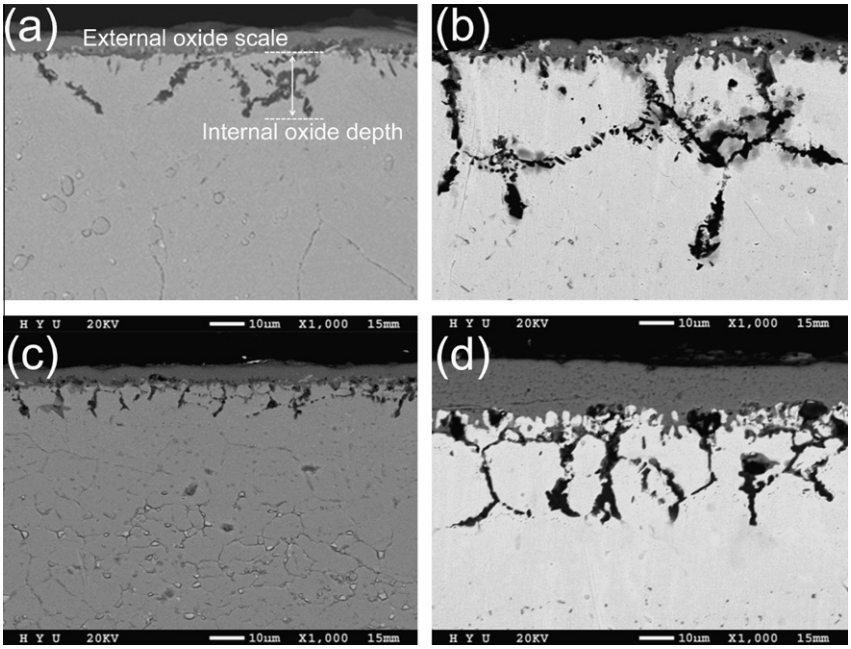

Fig. 1. Morphologies of the AR after aging at 950 °C for: (a) 120 h and (b) 2000 h and of the GR after aging at 950 °C for: (c) 120 h and (d) 2000 h in He atmosphere.

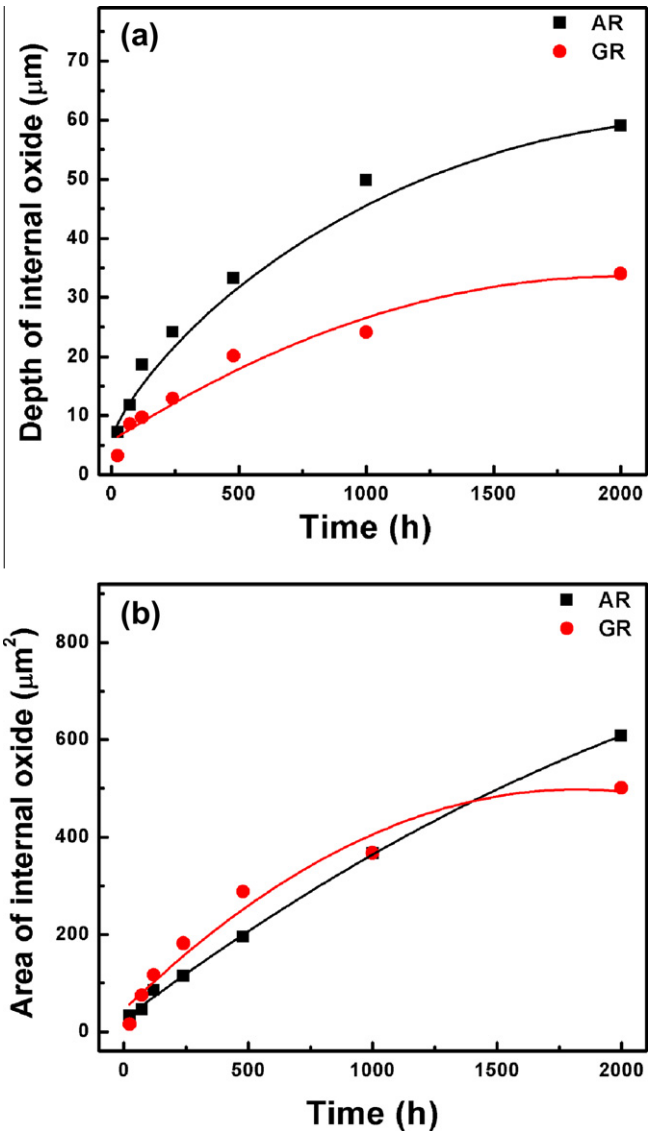

Fig. 2. Changes of: (a) depth of internal oxide and (b) area of internal oxide after exposure to He atmosphere at 950 °C.

ward the matrix in the Al-depleted zone. The Al concentration intensities were normalized to be the same value at $x = 0$ for apparent comparison of their gradients. In the case of AR, the Al concentration gradient was nearly sustained in spite of prolonged exposure from 480 h to 2000 h, while it became much smaller in GR. Thus, the supply of Al in AR remains almost the same for the internal oxidation after 2000 h. However, the internal oxidation rate became slower in GR since the Al concentration gradient became smaller due to the rapid oxidation during the initial exposure. Consequently, the internal oxidation in GR progressed rapidly during the initial exposure but it became slow at the prolonged exposure state.

3.2. Mechanical evaluation

Table 2 presents the Vickers hardness of AR and GR after aging at 950 °C for 2000 h. The Vickers hardness were 209 Hv for AR and 242 Hv for GR at the matrix in the middle of specimen. High hardness for GR was caused by grain size refinement. The Vickers hardness measured in the Cr-depleted zone below the internal oxidation region of AR and GR decreased to 203 Hv and 234 Hv, respectively. The depletion of the alloying elements, such as Cr and Al, caused the decreases in the solid-solution strengthening effect.

Also, the Vickers hardness test was applied to evaluate the degree of densely stretched internal oxide by a homogeneity indexing method. Fig. 4 demonstrates the distribution of the Vickers hardness at the internal oxidation region. The Vickers hardness test was carried out at regular intervals paralleling to external oxide scale in the internal oxidation region, as presented in an illustration of Fig. 4. To evaluate the degree of densely stretched internal oxide, a homogeneity index was calculated by the average Vickers hardness and standard deviation [17]

$$HI = \frac{S}{\overline{H}} \times 100 \tag{1}$$

$$S^2 = \frac{1}{n-1}\sum_{i=1}^{n}(H_i - \overline{H})^2 \tag{2}$$

Here, HI is the homogeneity index, S is the standard deviation, and $\bar{H}$ is the average of hardness. The distribution of the Vickers hardness was relatively narrow for GR comparing to that of AR. The standard deviation of Vickers hardness in AR and GR was confirmed as 27 and 24, respectively. The homogeneity index of GR (8.7) was lower than that of AR (11.9). As a result, it was confirmed that the internal oxide in GR was more densely stretched along the grain boundary.

Fig. 5 presents load–displacements obtained by 3-point bending test after exposure at 950 °C for 120 h. The input energy was calculated by the area of load–displacement curve. The total input energy of GR, 1903 mJ, was larger than that of AR, 1624 mJ, indicating that the strength of GR was improved by grain refinement.

Crack propagation behavior was also observed after the 3-point bending test. Generally, under external tensile stress, voids are generated at the interface between the matrix and the brittle internal oxide. By continuously applying stress, the generated voids can be made to coalesce, thereby forming cracks. Cracks are initiated at the internal oxide and propagated along the grain boundary [12]. Fig. 6 depicts crack morphologies under tensile stress after the 3-point bending test. Before the bending test, AR and GR specimens showed internal oxides with average depths of approximately 19 μm and 10 μm, respectively. As presented in Fig. 6, cracks over the average depth of the internal oxide in AR and GR were generated after the bending test. The crack in AR propagated deep along the grain boundary compared to that of GR because of a longer internal oxide. The matrix/internal oxide interface was more easily fractured by bending. Therefore, it is believed that the crack formed from the matrix/internal oxide interface acts as a defect under bending test, similar to a notch. According to Griffith [18], stress concentration increases with increasing crack length. The stress concentration in AR was higher than that in GR because of a longer internal oxide. Thus, a crack was initiated at the tip of the internal oxide via stress concentration and propagated along the grain boundary. The crack in AR propagated to a depth of around 150 μm due to relatively higher stress concentrations. On the other hand, short cracks below 40 μm were observed in GR due to comparatively lower stress concentrations. These short cracks were also generated widely by distribution of stress at the internal oxide because of the densely stretched internal oxide. Consequently, crack propagation at the tip of the internal oxide in GR was restricted by distribution of stress and reduction of stress concentration.

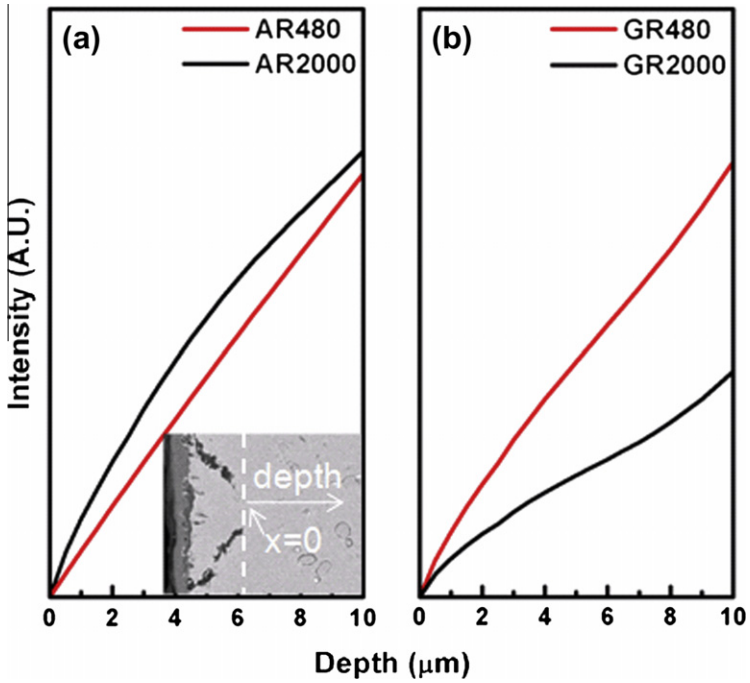

Fig. 3. The relative amount of Al concentration profiles for: (a) AR and (b) GR after exposure for 480 h and 2000 h in He atmosphere.

Table 2
The Vickers hardness changes of AR and GR after aging at 950 °C for 2000 h in He atmosphere.

	Vickers hardness (Hv)		
	Matrix	Cr-depleted zone	Internal oxidation region
AR	209	203	227
GR	242	234	276

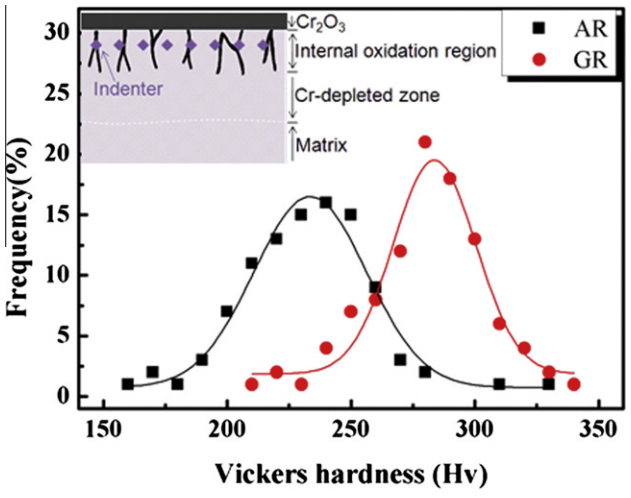

Fig. 4. The Vickers hardness curves of the internal oxide region after exposure to He atmosphere at 950 °C for 2000 h.

4. Summary

The oxide layer consisted of Cr_2O_3 in the external oxide scale and Al_2O_3 in the internal oxide was formed in AR and GR by exposure to high temperature in He atmosphere with some impurities. Internal oxides in both samples progressed along the grain boundary. These in GR were densely stretched compared to those of AR because of grain refinements. In addition, the average depth of the internal oxide region in GR was shorter than that in AR. The internal oxidation of GR rapidly increased during initial exposure and then gradually decreased by prolonged exposure, while AR showed a constant oxidation rate.

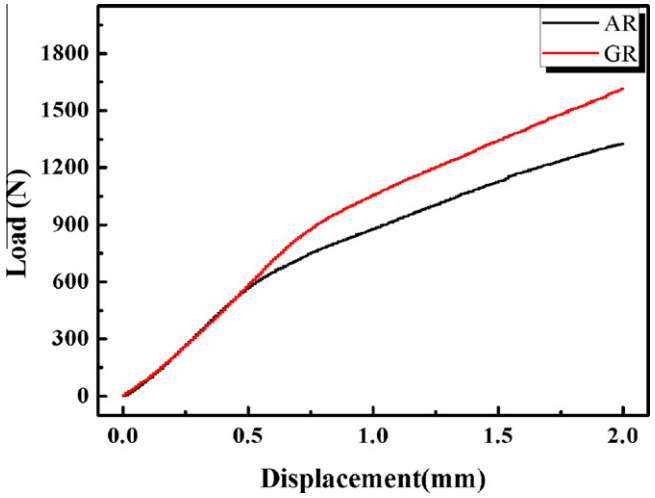

Fig. 5. Load–displacement curves by the 3-point bending test for AR and GR aged for 120 h in He atmosphere.

Cracks under external tensile stress were initiated at the tip of the internal oxide and propagated along the grain boundary. In the AR sample, larger crack were observed due to relatively higher stress concentration related to the longer internal oxide. In contrast, a number of short cracks in GR were dispersed close to each other in the near surface region due to distribution of stress and reduction of stress concentration related to more densely stretched, shorter internal oxides.

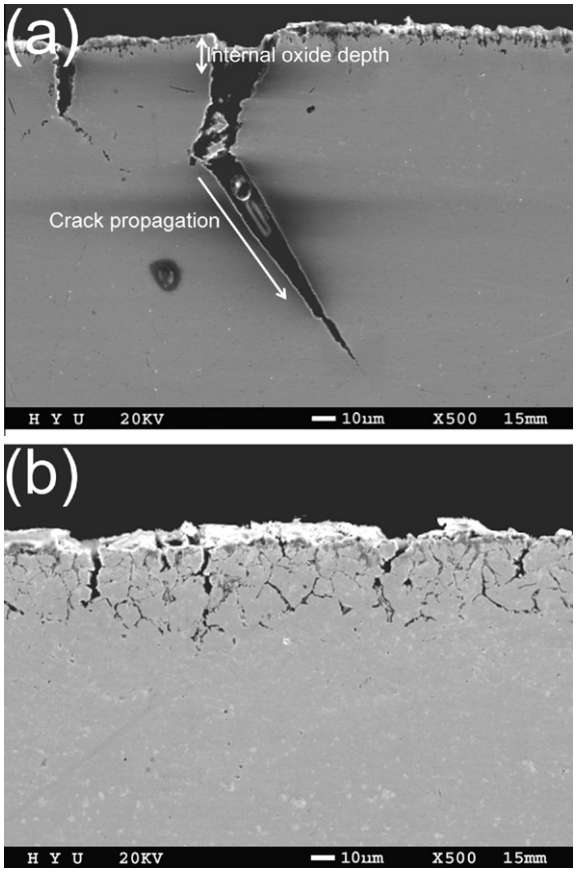

Fig. 6. Morphologies after 3-point bending test of: (a) AR and (b) GR aged for 120 h in He atmosphere.

Acknowledgments

This work was financially supported by Ministry of Education, Science and Technology (MEST) through the Nuclear Hydrogen Technology Development (NHTD) program.

References

[1] T.H. Bassford, J.C. Hosier, Nucl. Tech. 66 (1984) 35–43.
[2] S. Kihara, J.B. Newkirk, A. Ohtomo, Y. Saiga, Metall. Trans. A 11A (1980) 1019–1031.
[3] S. Rahman, G. Priyadarshan, K.S. Raja, C. Nesbitt, M. Misra, Mater. Lett. 62 (15) (2008) 2263–2266.
[4] R.K. Nanstad, D.A. McClintock, D.T. Hoelzer, L. Tan, T.R. Allen, J. Nucl. Mater. 392 (2009) 331–340.
[5] A. Kewther, B.S. Yilbas, M.S.J. Hashmi, J. Mater. Eng. Perform. 10 (2001) 108–113.
[6] L. Tan, K. Sridharan, T.R. Allen, R.K. Nanstad, D.A. McClintock, J. Nucl. Mater. 374 (2008) 270–280.
[7] L. Tan, X. Ren, K. Sridharan, T.R. Allen, Corros. Sci. 50 (2008) 3056–3062.
[8] J. Chapovaloff, D. Kaczorowski, G. Girardin, Mater. Corros. 59 (2008) 584–590.
[9] C. Cabet, J. Chapovaloff, F. Rouillard, G. Girardin, D. Kaczorowski, K. Wolski, M. Pijolat, J. Nucl. Mater. 375 (2008) 173–184.
[10] S.K. Sharma, G.D. Ko, F.X. Li, K.J. Kang, J. Nucl. Mater. 378 (2008) 144–152.
[11] D. Kim, C. Jang, W.S. Ryu, Oxid. Meter. 71 (2009) 271–293.
[12] H.M. Yun, P.J. Ennis, H. Nickel, H. Schuster, J. Nucl. Mater. 125 (1984) 258–272.
[13] B. Wilshire, C.J. Palmer, Scripta Mater. 46 (7) (2002) 483–488.
[14] T.S. Jo, S.H. Kim, D.-G. Kim, J.Y. Park, Y.D. Kim, Met. Mater. Inter. 14 (6) (2008) 739–743.
[15] C.T. Sims, N.S. Stoloff, W.C. Hagel, Superalloys II, John Willey & Sons, New York, 1987. pp. 293–326.
[16] N. Birks, G.H. Meier, F.S. Pettit, Introduction to the High Temperature Oxidation of Metals, second ed., Cambridge University Press, 2006. pp. 101–162.
[17] D.-G. Kim, G.-S. Kim, M.-J. Suk, S.-T. Oh, Y.D. Kim, Scripta Mater. 51 (2004) 677–681.
[18] A.A. Griffith, Philos. Trans. R. Soc. London Ser. A 221 (1920) 163–198.